Experimental study of a light high-speed train

Francisca Maria Pinto Salvador
francisca.salvador@tecnico.ulisboa.pt

Instituto Superior Técnico, Universidade de Lisboa, Portugal

December 2021

Abstract

The present work consists on a preliminary study of a light high-speed train's lateral stability, in the presence of strong winds. In order to evaluate how the aerodynamic coefficients vary in these conditions, wind tunnel experiments were performed as well as numerical simulations.

The experiments were done in an open test section of a closed circuit wind tunnel. Through an analysis of experimental errors, it was possible to obtain the variation of C_D, C_L and C_F with respect to Re and yaw angle, β. With the help of commercial software, Star-CCM+, numerical simulations, with RANS $k-\omega$ SST were performed. It was possible to obtain aerodynamic coefficients' variation with yaw angle, similar to the experimental ones.

To conclude the study, in order to justify the encountered differences between the simulated flow and the experimental flow, it was also analysed the pressure distribution for the numerical case.

Keywords Light high-speed train, lateral stability, CFD, wind tunnel

1. Introduction

The railway system brings numerous benefits to society, both social and economically. Since the appearance of the first high-speed train in 1964, in Japan, the interest for high-speed train's development has been increasing in various countries, Portugal included.

In [1] it is proposed a light high-speed train to operate in the Portuguese railway tracks. It was projected in order to constitute an advantage in social, economic and ambient aspects with regards to the current operating trains in Portugal. However, due to the operational high velocity range, some problems may arise regarding its aerodynamic performance, and it is of interest to understand the key features of the train and its implications in the presence of lateral winds.

1.1 Light high-speed train

The dimensions of the train are presented in Figure 1, with a transversal area of $7.9\ [m^2]$.

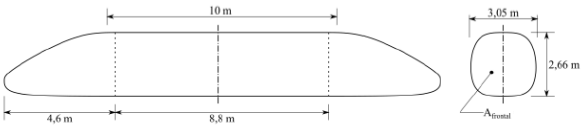

Figure 1: Light high-speed train geometry and dimensions

In comparison with conventional trains, the proposed one has reduced dimensions and it does not require the use of connecting elements between carriages (single car). So, although its lateral area reduction leads to a smaller lateral force, it presents a smaller tare weight, which can lead to lateral stability problems. In order to guarantee the passengers safety a thorough study was performed.

2. Experimental study

2.1 Wind Tunnel

The experimental studies were done at the Portuguese Air Force Academy (AFA), where there is a subsonic ($Ma < 0.8$), closed circuit wind tunnel.

This tunnel allowed velocities up to $70\ [\mathrm{m/s}]$, with a turbulent intensity smaller than $1[\%]$ and a velocity uniformity of $2[\%]$, [2]. The velocity was controlled through a control panel present in the tunnel, which automatically regulates the velocity using the static pressure measurement upstream and downstream of the contraction.

The test section can be open or closed. Nonetheless, technical limitations restricted the experimental study to using the open test section. When operating in these conditions, and since the aerodynamic balance cannot be in contact with the flow, a table was installed in order to obtain a solid boundary on the test section "floor".

2.2 Geometry

The geometry used during the experimental activity varied according to the encountered needs. Initially a geometry similar to Figure 1 was used, on a $1{:}\,15$ scale, designated by original geometry. After some experiments, the train's tale detached from the main body fuselage. While the new model was being produced, with the goal of filtering experimental errors, the modified (taleless) train was used in the meantime. This geometry is henceforth called modified geometry. The study was finalised by considering the new model, which presents a similar fuselage to the original one, with a new tale geometry, proposed in [3]. This was called optimized geometry and it was on a $1{:}\,17$ scale.

In an experimental context, it is necessary to have a connection between the train and the balance, guaranteeing the forces measurement. This connection element will be designated by support.

There was also the need to force the flow transition on the train nose, ensuring a dynamic similarity with the real case, which operates at all times on turbulent regime.

2.3 Operating conditions

During the experimental activities, it was detected a poor measurement of the velocity. So, a Pitot static system was installed. Due to the limitations of the manometer, the studied velocity ranged from 5[m/s] to 67,5 [m/s].

Provided that it was pretended to study the train's lateral stability for its real operating velocity of approximately 250 [km/h] and that the medium wind velocity Portugal for the past nine years is 43.2 [km/h], it would be sufficient to study the stability to yaw angles up to $10°$. Nevertheless, in order to have a safety margin, it was studied a yaw angle up to approximately $20°$.

2.4 Density and dynamic viscosity calculation

Since the density (ρ) and the dynamic viscosity (μ) vary with the temperature of the activity, it was required a correction of those values. Knowing the ambient temperature, $T_\infty\ [K]$, it is possible to obtain the saturated vapour pressure, $p_{sv}\ [Pa]$, using equation 1, from [4] :

$$p_{sv} = \exp\left(a_0\, T_\infty^2 + a_1\, T_\infty + a_2 + a_3\, T_\infty^{-1}\right) \quad (1)$$

With $a_i, i = 0, 1, 2$ and 3, constants presented in Table 1.

Using the relative humidity, ϕ [%], it is possible to calculate the water vapour pressure, using equation 2:

$$p_v = p_{vs}\,\frac{\phi}{100} \quad (2)$$

Assuming that specific humidity, $w\ [Kg_{H_2O}/Kg_{da}]$, is constant, it is possible to obtain its value from equation 3 and afterwards $\rho[\mathrm{kg/m^3}]$ from equation 4, both taken from [5]:

$$w = 0{,}62198\ \frac{p_v}{p_\infty - p_v} \quad (3)$$

$$\rho = \frac{p_\infty}{R_a T}\,\frac{(1+w)}{(1+1{,}6078\,w)} \quad (4)$$

With $R_a = 287{,}055\ [J/(Kg.K)]$, $T\ [K]$ the flow temperature and $p_\infty\ [Pa]$ the ambient pressure.

For the $\mu\ [Pa.s]$ calculation, equations 5, 6 and 7 were used:

$$f = a_0 + a_1\, p + a_2\, (T - 273.15)^2 \quad (5)$$

$$x_v = \frac{\phi}{100} \frac{p_{sv}}{p_\infty} f \quad (6)$$

$$\mu = (a_0 + a_1\, T + (a_2 + a_3\, T)\, x_v + a_4\, T^2 + \\ + a_5\, x_v^2\,) \times 10^{-8} \quad (7)$$

With f a multiplication factor, x_v the molar fraction of water vapour and a_i , $i = 0, 1, 2, 3, 4$ and 5 constants presented in table 1:

Table 1: Constants used for the calculations of p_{sv} , f and μ [4]

	a_0	a_1	a_2	a_3	a_4	a_5
p_{sv}	1,2378847E-5	-1.9121216E-2	33.93711047	-6.3431645E3	-	-
f	1.00062	3.14E-8	5.6E-7	-	-	-
μ	84,986	7	113.157	-1	-3.750E-3	-100,015

2.5 Dynamic pressure calculation

The dynamic pressure at the inlet of the test section was calculated using an inclined tube manometer. As the tube was vertical and calibrated to measure dynamic pressure in height of water column, the pressure was obtained from Equation 8:

$$p_{din} = \Delta h\ g\ \rho_{H_2O} \quad (8)$$

With $\Delta h\,[m]$ the height of water column, $g = 9{,}8005\ [m/s^2]$ the gravity acceleration in Sintra and ρ_{H_2O} the water density.

2.6 Aerodynamic coefficients calculation

In order to obtain the aerodynamic coefficients, equation 9 was used:

$$C_i = \frac{i}{p_{din}\, A_t}, \text{ with } \quad i = D, L\ e\ F \quad (9)$$

With D as the drag force, L the lift force and F the lateral force, measured with the aerodynamic balance. One import remark is that D was calculated in the flow direction, L perpendicular to D (vertical) and F normal to both vertical and longitudinal plane.

3. Experimental results

3.1 Original geometry

This geometry allowed for a preliminary analysis of the aerodynamic forces. The experimental tests started for null yaw angle. Initially the obtained values were too high. So, it was performed an alignment check of the train with the flow, varying the yaw angle. Having obtained results with no physical meaning, there was the possibility of the table interfering with the balance, making its measurements values vary, as seen in [2]. Wedges were used to stabilize the table and restrict its movement.

During one of the experimental activities, the tale of the train detached from the fuselage, due to poor glue quality. As stated previously, this modified model was used in the meantime.

3.2 Modified geometry

In the beginning there was an increase in temperature with the course of the experiments. The flow temperature was taken for each experiment as well as ambient conditions, and in the data process ρ and μ were adjusted for temperature and humidity, using the formulas presented in section 2.4.

It was not known whether the console was correcting the mass flow with the temperature increase, as so a Pitot tube was installed at the nozzle entry. From Bernoulli equation and having the pressure at the entry of the test section, it was also possible to determine the dynamic pressure. Having the dynamic pressure and density calculated as a function of the temperature and humidity for each experiment, one can now calculate the velocity in that section.

In Figure 2, the blue line represents the variation of the velocity calculated with the measured dynamic pressure, as a function of the velocity measured in the console.

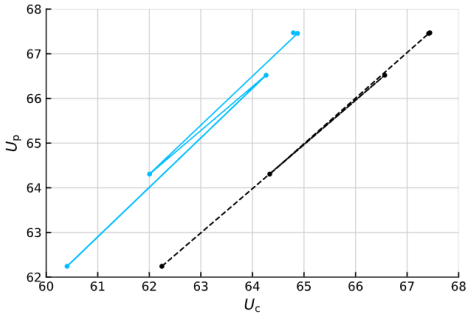

Figure 2: Velocity variation calculated from the manometer as a function of the console velocity. Blue line – before the correction; black line – after the correction.

Analysing the graph presented above, it is possible to infer that the velocity calculated through the height of water column, U_p, differs from the one measured from the console, U_c. It was expected a linear variation, as such it was then evaluated if this evolution resulted from the temperature differences verified during the experiments.

Using equation 10, and assuming the areas ratio is correctly computed, as well as the pressure measurement in these sections, it comes:

$$U_{c_{corr}} = U_c \left(\frac{\rho_c}{\rho}\right) \quad (10)$$

With $U_{c_{corr}}$ the corrected console velocity, ρ_c the density used for the computation of console velocity (through iterative process) and ρ the density as a function of temperature and humidity.

Comparing $U_{c_{corr}}$ and U_p, from the plot (black line in Figure 2), it is possible to verify the initial hypothesis of the console considering a constant density.

A new series of experiments were performed, calculating the velocity from the dynamic pressure measurements. Figure 3 presents the coefficients obtained as a function of Re.

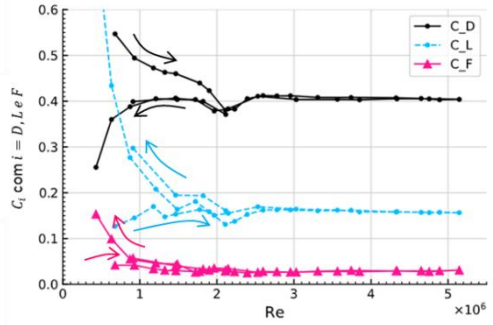

Figure 3: Aerodynamic coefficients with Re for $\beta = 0°$, with the arrows indicating the sequence of velocity increase followed by its decrease.

It was verified, for Re in the range $1.8\text{E}6$ to $2.5\text{E}6$, an irregularity in C_D, which seems to indicate flow transition. However, when decreasing the velocity in the experiments, the irregularity was also verified for the same Re range, which might indicate that the irregularity does not represent transition. Note that since the flow is in the turbulent regime, even with a decrease in velocity, it is expected that the flow stays in the turbulent regime.

When decreasing the velocity, for Re smaller than $1\text{E}6$, C_D decreased, which was not the expected behaviour.

For both C_L and C_F the irregularity is not as evident as for C_D, however when decreasing the velocity, for smaller Re its values significantly increase. This suggests an error during the measurement. A new experiment was performed, in order to avoid the Re range where the irregularity was verified, Figure 4.

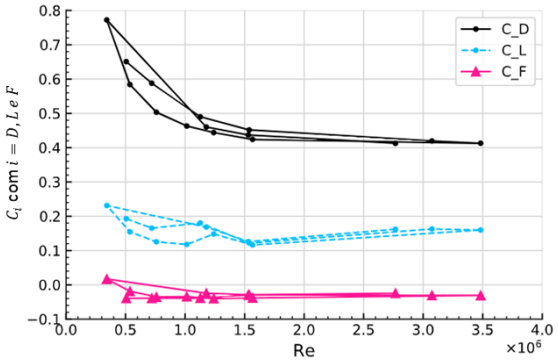

Figure 4: Aerodynamic coefficients with Re, avoiding the irregularity range, for $\beta = 0°$

From Figure 4, it is possible to verify the typical behaviour that decreasing Re has in the coefficients (C_L and C_D decrease with Re and C_F is approximately constant, although not null). It suggests the flow is completely turbulent.

Furthermore, the previous observed behaviour when decreasing velocity was not obtained for this experiment. For Re in the range $1.8\text{E}6$ to $2.5\text{E}6$, the table and its surrounding vibrated quite visibly, which might have moved the model from its original position, resulting in the observed behaviour for smaller Re in Figure 3. Let us now try to understand the reason for such depression in the C_D curve.

Since the anomaly coincides with the Re range in which vibration was encountered, two reasons were analysed:

(A) The aerodynamic balance is sensible to vibrations and for this, don't have a linear calibration curve, resulting in different forces values from the measures ones;

(B) The tunnel or aerodynamic balance resonance.

3.2.1 Case (A)

This was verified through the base pressure measurement of the train. However, in a similar behaviour for the same Re range, the irregularity was present (Figure 5).

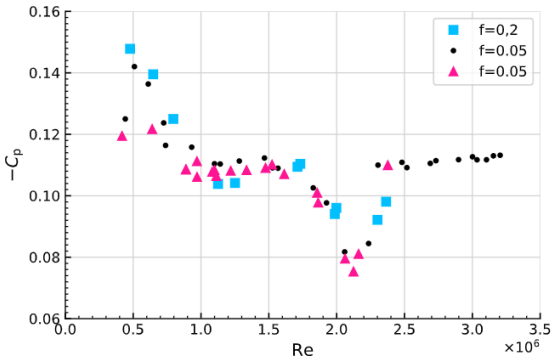

Figure 5: C_p as a function of Re for diferente values of f, with f a conversion factor of the manometer as a function of its angle

3.2.2 Case (B)

Considering for the Re range in question, the jet free shear layer hits the tunnel with a frequency similar to tunnel's natural frequency, making it resonate. As a results, the tunnel has low frequency pulsations, which can affect the measurements of the aerodynamic forces, as seen in [6]. Note that as the tunnel begins to resonate, there are velocity and pressure fluctuations, making the coefficients vary.

One other important source of error might be the aerodynamic balance having a natural frequency similar to the natural frequency of the tunnel.

Due to the importance of this phenomena, it is suggested a future study of the tunnel's natural frequency and how it can influence the force measurements, like [6]. Some possible ways to avoid resonance are experiments in a closed test section; the use of honeycombs at the exit of the test section; to adopt the proposed methodology in [6].

For all other experiments, the range of velocities where tunnel vibration was encountered was avoided.

This geometry study was finalised with an attempt to reconstruct the model, although, not successfully, since C_D was equal to the value without the tale, which suggests no pressure recovery and fully separated flow. It is possible to conclude that during the attempted reconstruction, the angle of the tail and main body fuselage is an important factor for this study.

3.3 Optimized geometry

Experiments were performed with and without the table. Given the significant difference between the results, it was possible to confirm the table importance in an open section wind tunnel. On the other side it was possible to verify a decrease in C_L as expected due to ground effect.

During these new experiments, some error sources were identified:

- centred table effect: since the flow below the train has a relative pressure different than zero, and below the table pressure is atmospheric, it is predictable that there is flow entering or leaving, whether the pressure difference is negative or positive, respectively. If the table opening is not fully aligned/centred with the aerodynamic balance it influences the flow velocity;
- increase in the drag as a result of the support presence.

New experiments were performed with the table centred and aligned as precise as possible, with the obtained results present in Table 2:

Table 2: Coefficients for different β

β	C_D	C_L	C_F
-10º	0,266	0,700	0,575
-5º	0,170	0,320	0,285
0º	0,148	0,185	0,052
5º	0,160	0,259	-0,176

All coefficients have an evolution with the yaw angle, as expected. However, it was verified that a small table misalignment completely affected the results. Thus, in order to try to control the flow obstruction resultant from the cavity, a wrapper was used around the balance. The results are present in Figure 6.

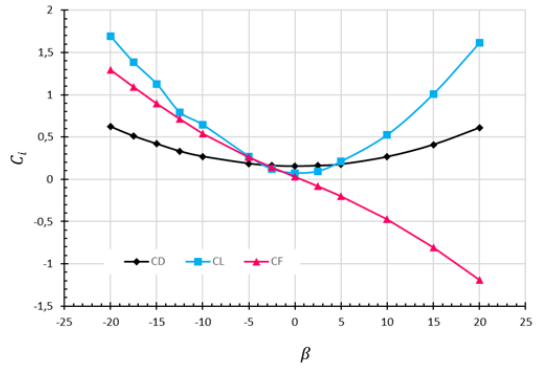

Figure 6: Coefficients with yaw angle, with the wrapper

It is possible to observe that C_F has an evolution as expected: null for null yaw angle and increases in module, with the module of the angle. Furthermore, C_L and C_D present as expected, a minimum for null yaw angle and its value increase with the absolute value of β.

Comparing results with and without the wrapper, it is possible to infer the wrapper does not have a significant influence on C_D. The opposite was verified for C_L and C_F. In particular, C_F was smaller for every angle.

To conclude this study, it was also analysed the temperature influence on C_D. This difference appears to be justified by the temperature difference between the model and the flow. Note that in these circumstances the boundary layer, BL, is not at flow temperature affecting the viscous properties of air in that region, hence it alters the model's friction drag coefficient.

4. Numerical study

The numerical study was performed with help of commercial software Star-CCM+ and consisted on studying the optimized geometry. The model, at real scale $(1:1)$ was imported for the program and a series of steps, which will be presented next, were followed.

4.1 Domain and boundary conditions

After importing the model, it was defined a parallelepiped domain, whose dimensions were determined through a series of iterative processes, with exception of train height relative to the domain's base. This was determined according to the height of the experimental model to the floor, 1.6 [m].

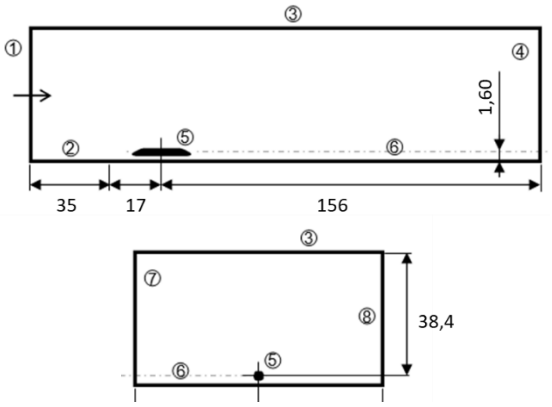

Figure 7: Dimensions and boundaries of the domain.
1 – Inlet; 2 – Base with $\tau_w = 0$; 3 – Top; 4 – Outlet;
5 – Train; 6 – Base with $U_w = 0$; 7/8 - Laterals

The boundary conditions were also defined in order to be as close as possible to the experimental conditions. Thus it was possible to define velocity inlet condition in face 1 and pressure outlet in face 4; symmetry plane in both top and laterals, no slip wall condition in the train and base, and slip-wall condition for face 2.

4.2 Mesh

An unstructured, polyhedral mesh was generated for the entire domain. After defining its base size, 4 refinement volumes were generated, close to the train as in Figure 8.

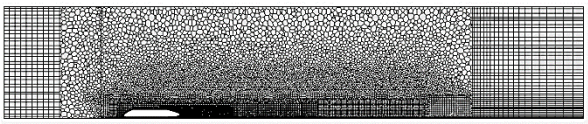

Figure 8: Refinement volumes

There was also created extrusion blocks at the inlet and outlet, with the goal of obtaining a more representative computational domain without significantly increasing computational demand.

To correctly represent the BL close to the wall, a prism layer mesh was used. To obtain a larger precision, wall function were not used, meaning, shear stress at the wall is calculated by definition:

$$\tau_w = \mu \frac{\partial U}{\partial y}\Big|_{y=0} \quad (11)$$

with U being the velocity, y the vertical distance and μ the dynamic viscosity.

To properly solve the linear sublayer region, the dimensionless wall distance (y^+) must be smaller than 1. Since y^+ is given by equation (12), it is possible to calculate Δy_1 (near wall prism layer height), with u_τ the friction velocity.

$$y^+ = \frac{\rho\, u_\tau\, \Delta y_1}{\mu} \quad (12)$$

To calculate the friction velocity, it was assumed a fully turbulent flow and for a first estimate equations 13 (turbulent flow over a flat plate), 14 and 15 were used:

$$C_f = 0.058\, Re_L^{-0.02} \quad (13)$$

$$\tau_w = \frac{1}{2}\, C_f\, \rho\, U_\infty^2 \quad (14)$$

$$u_\tau = \sqrt{\frac{\tau_w}{\rho}} \quad (15)$$

Assuming turbulent flow from the train's nose, von Kármán equation was used to estimate the total height of the prism layer δ, equation 16.

$$\delta = \frac{0{,}37L}{Re^{0.2}} \quad (16)$$

Even though these values were used only for a first estimate, it immediately gave $y^+ < 1$, so an iterative process was not adopted.

The total number of prism layers (N) controls the number of layers present in the prism layer mesh. It must be large enough, in order to have enough layers in each zone to properly discretize the boundary layer zones independently. The final value was chosen to be N=20, with hyperbolic tangent as stretching function, in order to have a smooth transition between the layers further from the wall.

4.3 Numerical calculations

Numerical calculations were performed using Star-CCM+. RANS model with turbulence model $\mathrm{k}-\mathrm{w}\ \mathrm{SST}$ was used. The governing equations were linearized in an implicit manner, with segregated flow solver.

In the spatial discretization, second-order upwind and Hybrid Gauss-LSQ were chosen, with the limiter, by default, chosen to be the Venkatakrishnan. For unsteady simulations, Implicit Unsteady model was the option chosen. Initially the CFL number was kept equal to 1 and iteratively increased until 10.

4.4 Initial conditions

To guarantee dynamic similarity between the numerical and experimental flow, it was necessary to guarantee that $Re_{exp} = Re_{num}$.

Since the numerical model is at real scale, to obtain the same similarity conditions it was decided to consider the same velocity and change the fluid viscosity to be 17 times higher than the real fluid viscosity.

5. Numerical results

5.1 Verification

In order to estimate the numerical uncertainty of a given variable, the solution verification was done using the method proposed in [7]. Hence, it was possible to obtain the aerodynamic coefficients variation as a function of the grid refinement ratio, as seen in Figure 9.

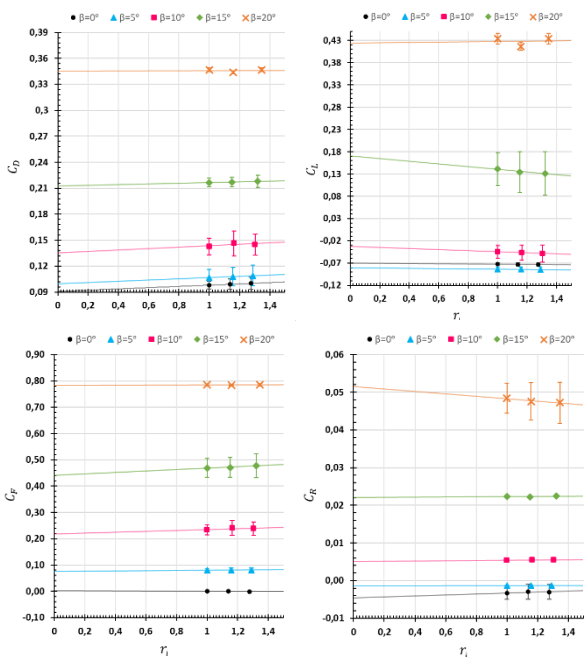

Figure 9: Aerodynamic coefficients as a function of gric refinement ratio

The results obtained for the uncertainty were as expected, with exception for the $\beta = 20°$. Since its value is practically invariant with r_i, it is probable that the mesh is too coarse, giving a bad prediction of ϕ_0 (exact value) and consequently of its uncertainty. The same goes for rolling coefficient, C_R. Having said this, the study of C_R and $\beta = 20°$ was not performed.

5.2 Validation

In order to estimate the uncertainty of the numerical model, the method proposed in [7] was used to validate the results. Figure 10 presents the variation of coefficients with β for both numerical and experimental cases.

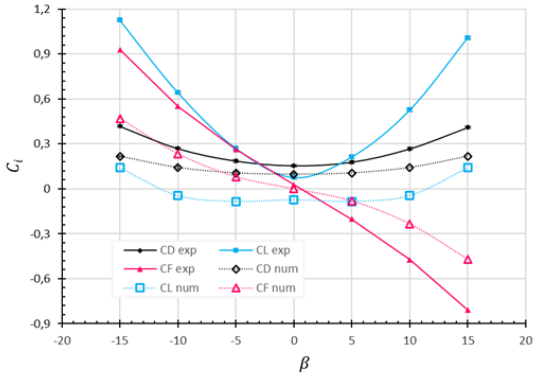

Figure 10: Aerodynamic coefficients with β

It was verified a numerical error of the same order of magnitude as the experimental error. Decreasing the modelling uncertainty will result from a decrease in both experimental error and numerical error. To conclude the verification procedure, it was used the definition of comparison error as a function of β presented in Figure 11.

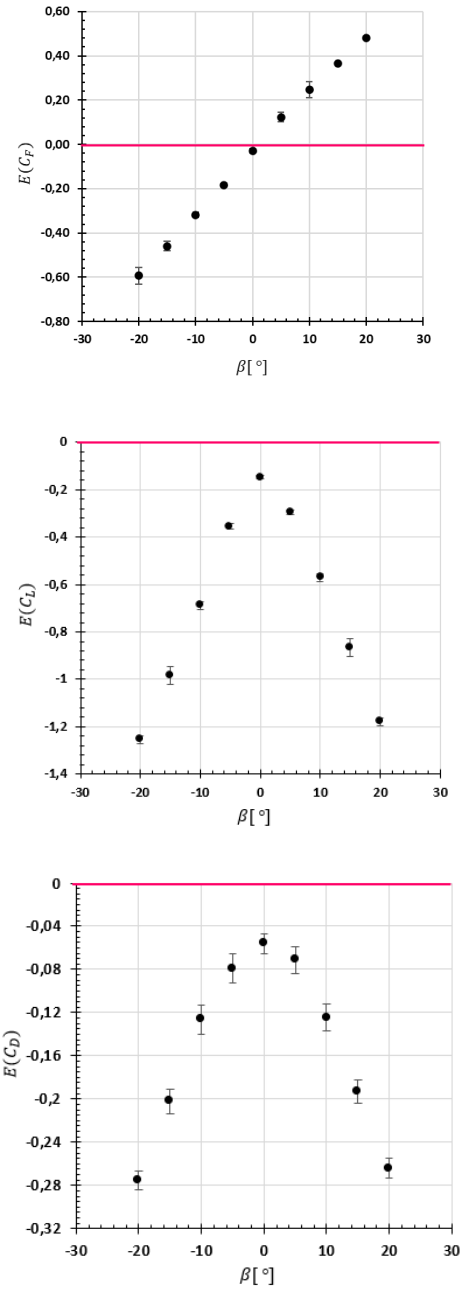

Figure 11: Comparison error of aerodynamic coefficients as a function of β

The modelling error, δ_{model}, is negative for C_D and C_L, leading to an underestimation. For C_F, δ_{model} is positive for positive angles and negative for null or negative angles.

It is also possible to verify an increase in the comparison error as the yaw angle increases.

6. Flow analysis

The flow pressure field study might give a more in depth answer to what was described in the previous section. Figure 12 presents the pressure distribution for the different studied yaw angles.

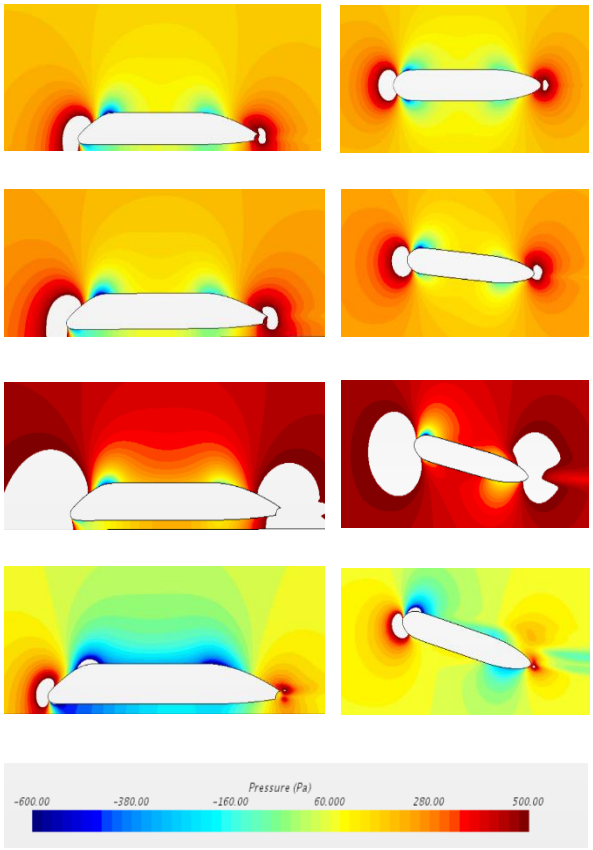

Figure 12: Pressure distribution as a function of β

With the increase in yaw angle, it is possible to see the dislocation of the stagnation point. As a result, due to the train's fuselage curvature, there is an increase in pressure on the windward side and the displacement of the suction peak to leeward side. This way, with the increase in β the pressure decreases in the leeward side and increases in the windward side, resulting in a increase of lateral force and consequently C_F.

The evolution of C_D with β is easily identified by the asymmetry of pressures previously described. Note that this asymmetry in pressure distribution as a result of displacement of the suction peak, and also as a result of separation occurring in the leeward side, has an impact on aerodynamic drag.

With the increase in β it is possible to identify a variation in the pressure field above the train. For yaw angles of $0°$ and $5°$, the pressure field is similar, leading to a similar lift force and consequently small variation in C_L. The low pressure under the train, resulting from the ground effect, appears to be similar to the pressure obtained above the train, with exception for the nose and tail. Note that in the nose there is a high pressure field as a result of the stagnation pressure and a low pressure field as a result of the suction peak, due to the curvature. Given that C_L is slightly negative, one can predict the effect of high pressure of the nose to overcompensate the lift force generated by the suction peak.

For $\beta = 10°$ there is an increase in the pressure field as a whole and consequently between the train and the ground. Hence, one can predict the lift force generated due to low pressure from suction peak to be more pronounced, giving a higher C_L than the previous cases.

For $\beta = 15°$ there is an increase in the suction peak on the top of the train and a significant decrease in pressure not only above the train but also between the train and the floor. Analysing the differences between the pressure on top and bottom of the train, it is possible to confirm the pressure above the train is smaller, giving origin to a positive lift force.

It is of interest to understand the differences encountered between both numerical and experimental cases. Two differences were found: the presence of the support in the experimental study and the presence of the cavity between the table and the aerodynamic balance (it has already been stated the importance of the cavity).

Although it is possible to predict that the pressure field will be influenced by the presence of

both, it is difficult to predict how much it will influence the flow.

7. Conclusions

With the present work results it is possible to conclude that numerical and experimental results have identical behaviour with the increase of yaw angle, even though the results are quite distinct. This arose from the differences in the experimental and numerical conditions, namely the presence or absence of the support and the presence of the cavity below the train, in the experimental activities

One of the goals of this work consisted in a preliminary study of the train's lateral stability in the presence of lateral winds at high velocities. However, it is not possible to conclude anything in regards to it, given that is was not possible to verify the similarity between the numerical and experimental solutions. Note that after the validation of the numerical model an approximation of the aerodynamic coefficients value can be obtained for a velocity close to the train's operational velocity, as long as $Ma < 0.8$.

Future studies should be performed in order to improve the similarity between the numerical and experimental cases

8. References

[1] J. André, Transporte Interurbano em Portugal, volume 1, IST Press, 2008.

[2] M. Wermans, "Caracterização do Túnel Aerodinâmico da Academia da Força Aérea," *Revista Científica Academia da Força Aérea,* vol. 10, pp. 67-81, 2020.

[3] C. Izidoro, "MSc. Thesis: Desafios Aerodinâmicos de um Comboio Ligeiro de Alta-Velocidade".

[4] K. Rasmussen, "Calculation methods for the physical properties of air used in the calibration of microphones," 1997.

[5] American Society of Heating, Refrigeration and Air Conditioning Engineers, ASHRAE Handbook, 1986.

[6] H. von Heesen e S. Wallmann, "Wind Tunnel Pulsations and Their Active Supression," *SAE Technical Paper Series,* 2000.

[7] L. Eça e M. Hoekstra, "A procedure for the estimation of the numerical uncertainty of CFD calculations based on grid refinement studies," *Journal of Computational Physics,* vol. 262, pp. 104-130, 2014.